Successful grafting of isolated molecular Cr_7Ni rings on Au(111) surface

V. Corradini,[1,*] F. Moro,[1,2] R. Biagi,[1,2] V. De Renzi,[1,2] U. del Pennino,[1,2] V. Bellini,[1] S. Carretta,[1,3] P. Santini,[1,3] V. A. Milway,[4] G. Timco,[4] R. E. P. Winpenny,[4] and M. Affronte[1,2]

[1]*INFM-CNR S3, National Research Centre, 41100 Modena, Italy*

[2]*Dipartimento di Fisica, Università di Modena e Reggio Emilia, via G. Campi 213/A, 41100 Modena, Italy*

[3]*Departimento di Fisica, Università di Parma, Viale G. P. Usberti 7/A, I-43100 Parma, Italy*

[4]*School of Chemistry, University of Manchester, Oxford Road, Manchester M13 9PL, United Kingdom*

(Received 6 March 2009; published 16 April 2009)

We deeply investigated the properties of submonolayer distributions of isolated molecular Cr_7Ni rings deposited on Au(111) by liquid phase. X-ray absorption spectra measured at the Cr and Ni $L_{2,3}$ edges show that the grafting of the Cr_7Ni rings onto the gold surface does not affect the oxidation state and the local symmetry of the Cr and Ni sites. The circular dichroism shows a change in sign of the Ni magnetic moment. This is due to a reduction in the exchange coupling constants that, however, preserves the structure of the low-energy levels of the grafted rings, as corroborated by spin-Hamiltonian simulations and comparison with measurements on bulk sample. Density-functional theory calculations show that the Ni-Cr bond gets weaker with slight ring distortion suggesting possible explanation for the observed magnetic behavior. These results show that complex magnetic molecules can be grafted onto surfaces, and that changes in their magnetic behavior must be examined in individual cases.

DOI: 10.1103/PhysRevB.79.144419 PACS number(s): 75.50.Xx, 61.46.Bc, 78.70.Dm, 87.64.ku

I. INTRODUCTION

Molecular nanomagnets (MNM) are molecules or nanoparticles comprising clusters of magnetic metal ions tightly coupled to each other by exchange interactions. Magnetic molecules have a discrete spectrum of energy levels that can be resolved at sufficiently low temperatures and eventually lead to the occurrence of quantum phenomena.[1] Mn_{12}ac is probably the most popular example of *high spin* molecular magnets but, recently, antiferromagnetic molecules with *low spin* have also attracted much interest. So far, most of the studies have been performed on bulk samples comprising collections of molecules packed in crystalline structures and generally weakly interacting to each other. Yet, this fact alone does not guarantee that the behavior observed on bulk crystals can be observed in all circumstances and one may wonder to which extent the environment may change, directly (chemically, electronically) or indirectly (structurally, magnetically, thermally) the molecular properties on different energy scales. This is a crucial issue in view of ultimate applications of single molecular units. The situation of isolated molecules on a surface is particularly intriguing and one may think to exploit the substrate to eventually tune the properties of the molecules.[2]

Much effort has been devoted so far to graft and study Mn_{12} on a surface using direct[3–5] and indirect grafting procedures.[6,7] While the thick films (TFs) behavior still resembles that of the bulk, recent results show that the influence of the substrate, together with a high chemical reactivity and sensitivity to the x-rays, induces heavy changes in a submonolayer (sML) of isolated Mn_{12} molecules on gold and Si, thus compromising their magnetic behavior.[4,5,8] Such drastic modifications, however, cannot be generalized to all MNM since molecules have different chemical reactivity and physical features.

Here we focus on molecular antiferromagnetic Cr_7Ni rings which are a new class of MNM on which interesting quantum phenomena have been observed[9,10] and that have been recently proposed as candidates for the implementation of quantum gates.[11,12] Cr_7Ni contains seven Cr^{3+} and one Ni^{2+} ions and the antiferromagnetic coupling leads to a molecular $S=1/2$ spin ground state at low field.[13,14] The presence of one isolated divalent ion (Ni^{2+}) in the Cr^{3+} wheel is particularly relevant since it allows the local magnetization to be probed, an essential aspect to study antiferromagnetic correlations. We recently reported the design of sulfur functionalized derivatives and the procedure to obtain, from solution, sML distributions of such Cr_7Ni rings grafted on Au(111).[14,15] The next, crucial step is to ensure that the chemical, electronic, and magnetic properties of grafted molecules remain equivalent to those observed in bulk. Only very few works have been published so far on the magnetic characterization of sML of such complex molecular systems[2,5] due to difficulties in defining deposition protocols and in finding suitable experimental techniques. Here we show that x-ray Absorption Spectroscopy (XAS) and magnetic circular dichroism (XMCD) are very powerful techniques to study molecular antiferromagnets because of their high sensitivity and to their element and shell selectivity.

We have studied four different Cr_7Ni derivatives deposited in the form of both microcrystalline thick films, representative of the bulk, and submonolayer distributions of isolated molecules (sML) deposited on Au(111). The investigated derivatives are: (1) Cr_7Ni-piv, i.e., the pristine compound; (2) Cr_7Ni-3tpc, with 16 thiophene ligands; (3) Cr_7Ni-4mtpp, with one peripheric 3-(4-methylthiophenyl) propionate ligand; (4) Cr_7Ni-phenoxy, with 16 phenoxybenzoate ligands (no sulfur). The four structures are shown in Fig. 1 and the synthetic procedures are described in the Appendix.

II. EXPERIMENTAL TECHNIQUES

The sML samples were obtained by immersing the Au(111) or Au/mica flamed-annealed surface in a mM solu-

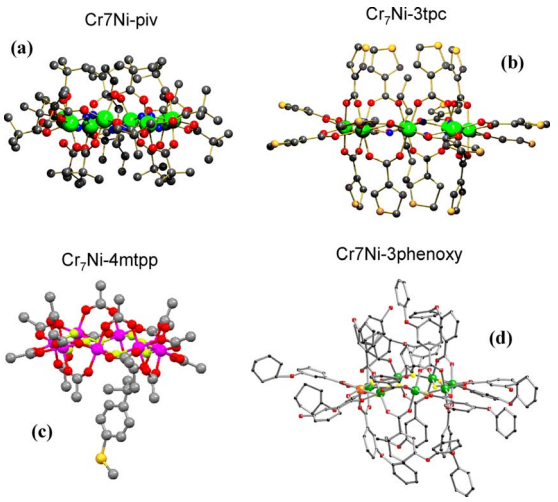

FIG. 1. (Color online) The structure of the four derivatives studied: (a) the not functionalized Cr_7Ni-piv ring, (b) the Cr_7Ni-3tpc with 16 TP ligands, (c) the Cr_7Ni-4mtpp with one 3-(4-methylthiophenyl) propionate (*S*-protected ligand), (d) the Cr_7Ni-phenoxy with 16 Phenoxybenzoate ligands (without *S*).

tion of the specific derivative. After the adsorption process the samples were rinsed with proper solvent in order to remove the excess of molecular layers, and quickly introduced in the experimental chamber. All the deposition parameters were optimized in order to get homogeneous submonolayers of spatially isolated molecules. Concentration of 5 mM and incubation time of 10 min were used for all the compounds while a tetrahydrofuran solvent was used for Cr_7Ni-piv, Cr_7Ni-3tpc, Cr_7Ni-4mtpp and a nonpolar solvent, dichloromethane, was used for Cr_7Ni-phenoxy. Scanning tunneling microscopy (STM) (see Fig. 2) and x-ray photoemission spectroscopy (XPS) were used to check that the desired two-dimensional distribution of nanometric entities was actually obtained. TFs were drop cast on a substrate starting from the saturated solution on highly oriented pyrolytic graphite (HOPG) substrate.

The XMCD experiments were carried out at the ID8 beamline of the European Synchrotron Radiation Facility (ESRF) in Grenoble (France). The lowest sample temperature reached was about 10 K and the base pressure of the

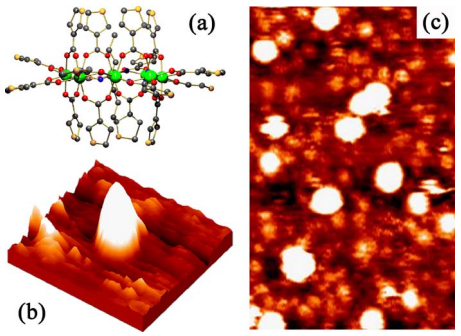

FIG. 2. (Color online) (c) STM image (50×25 nm^2) and (b) 3D view (13×13 nm^2) of a single Cr7Ni-3tpc cluster grafted on Au(111) surface. (a) Structure of the Cr7Ni-3tpc ring viewed perpendicularly to the Cr_7Ni plane.

experimental chamber 1.0×10^{-10} mbar. The photon source was an Apple II undulator that delivers a high flux of polarized light. We paid much attention to avoid any sample degradation induced by radiation exposure, working with very low flux (below 10^{12} photons/s) and by strictly monitoring XAS spectra throughout all the experiments for detecting even the smallest traces of sample damaging.

XMCD measurements at the Cr and Ni $L_{2,3}$ edges were performed in total electron yield mode using circularly polarized light with about 100% polarization rate and with external magnetic field $\mu_0\mathbf{H}$ up to 5 T applied perpendicularly to the sample surface and parallel to the incident photon beam. The dichroic spectrum is the difference between the XAS spectra taken with the helicity of the incident photon (**P**) antiparallel ($\sigma^{\uparrow\downarrow}$) and parallel ($\sigma^{\uparrow\uparrow}$) to the sample magnetization (**M**). In order to minimize the effects of field inhomogeneity, we first fixed the field and switched the polarization parallel and antiparallel, then we made the same with the field in opposite direction. The $\sigma^{\uparrow\uparrow}$ ($\sigma^{\uparrow\downarrow}$) absorption spectra are the mean value of the spectra collected with the helicity parallel (antiparallel) to the sample magnetization.

III. RESULTS AND DISCUSSION

A. XAS and XMCD

In Fig. 3 the Cr (left) and Ni (right) $L_{2,3}$ XAS and XMCD spectra, measured at 5 T and 10 K for the three sMLs and for the Cr_7Ni-3tpc TF, are compared with that of the nonfunctionalized Cr_7Ni-piv TF.[16] In all sMLs and TFs, the XAS and XMCD spectral line shape are very similar (apart from the sign of the Ni dichroism that will be discussed below). The Cr absorption spectra present eight features characteristic of Cr^{3+} in O_h environment,[17] whereas the Ni XAS presents two peaks at the L_3 edge and a partially resolved doublet structure at the L_2 edge, characteristic of a high-spin Ni^{2+} ion in O_h environment.[18] Since the spectra of all the TFs perfectly reproduce those of the Cr7Ni-3tpc presented in Fig. 3, it is evident that the different functionalizations do not affect the core electronic structure of the ring. In addition, we emphasize that Cr and Ni $L_{2,3}$ absorption spectra for all the sMLs closely resemble those of the TFs. This shows that, within the (high) sensitivity of the technique and independently of the ligand type, the grafting onto the gold surface does not affects the valence electronic structure of the Cr and Ni ions: oxidation state, local environment, and crystal-field intensity at the Cr and Ni sites are not altered.

B. Ligand field multiplet calculations

XAS and XMCD spectra are simulated by using the ligand field multiplet model implemented by Thole.[19,20] The calculation takes into account spin-orbit coupling and treats the environment of the absorbing atom through the crystal-field parameters ($10Dq$, Ds, and Dt). The Slater integrals and the $2p$ and $3d$ spin-orbit interactions in the initial ($F^2_{dd}, F^4_{dd}, \zeta_{3d}$) as well as in the final states ($F^2_{dd}, F^4_{dd}, F^2_{pd}, G^1_{pd}, G^3_{pd}, \zeta_{2p}, \zeta_{3d}$) are calculated. Then the solid is simulated by adding a crystal-field Hamiltonian as a perturbation of the atomic result and projecting the $SO3$ into any desired point-group symmetry. In O_h symmetry, the $3d$ level is split

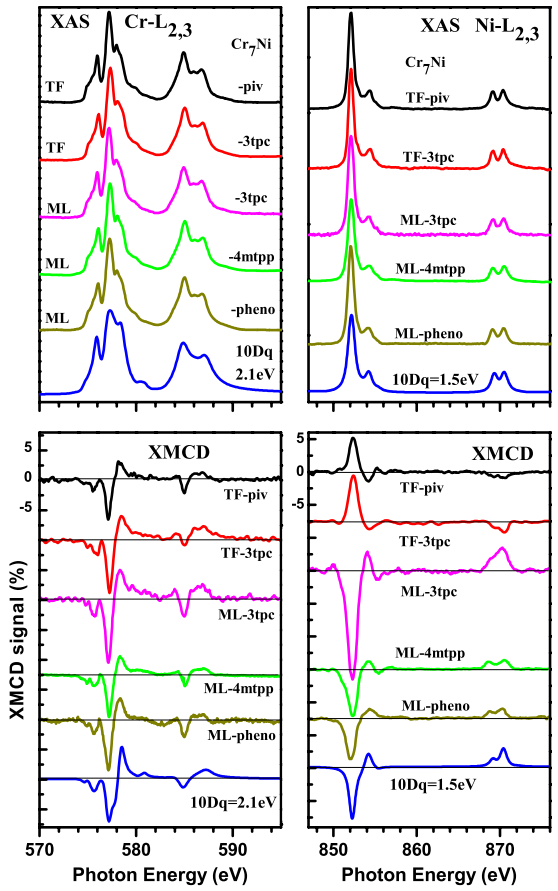

FIG. 3. (Color online) Cr (Left panel) and Ni (right panel) $L_{2,3}$ XAS and XMCD spectra for the Cr_7Ni-piv TF, Cr_7Ni-3tpc TF and sML, Cr_7Ni-4mtpp and Cr_7Ni-phenoxy sMLs at 10 K and 5 T, compared with the ligand field multiplet calculations: $10Dq=2.1$ eV for Cr^{3+} and $10Dq=1.5$ eV for Ni^{2+}, Lorentzian ($W_{L3}=0.2$ eV and 0.4 eV, $W_{L2}=0.6$ eV and 0.4 eV for Cr and Ni, respectively) and Gaussian ($W_G=150$ meV) broadening.

into e_g and t_{2g} orbitals with separation energy of $10Dq$. A further lowering of the symmetry to D_{4h} splits the orbitals by the additional Ds and Dt parameters.

We calculate the $L_{2,3}$ absorption edges for the Ni^{2+} and Cr^{3+} ions. The transitions involved in the atomic calculation are: $2p^63d^8 \rightarrow 2p^53d^9$ and $2p^63d^3 \rightarrow 2p^53d^4$ for the Ni^{2+} and Cr^{3+}, respectively. The Slater integrals were reduced of the 20% of the Hartree-Fock values to include the hybridization effects. In the crystal-field approach we describe the local symmetry of both Ni^{2+} and Cr^{3+} ions by tetragonal D_{4h} symmetry. Scanning through the ligand field parameters, (assumed equals for initial and final states) we find a good agreement between the experimental and theoretical spectra by considering the ions in O_h symmetry: $Ds=Dt=0$, $10Dq=2.1$ eV for Cr^{3+} and $Ds=Dt=0$, $10Dq=1.5$ eV for Ni^{2+}. This means that in all the Cr_7Ni systems the slightly distorted octahedral environment around the Cr and Ni ions can be safely approximated to an almost perfect octahedron. Table I summarizes the parameters used in the calculations.

The calculated spectra at the $L_{2,3}$ edges, shown in Fig. 3 of the paper, are convoluted with Lorentzian ($W_{L3}=0.2$ eV and 0.4 eV, $W_{L2}=0.6$ eV and 0.4 eV for Cr^{3+} and Ni^{2+}, respectively) and Gaussian ($W_G=150$ meV) broadening to simulate the core hole lifetime and the experimental resolution. The random orientation of the molecules requires to perform angular averages of the absorption cross section for all possible orientations of the magnetic field with respect to the molecular axes. This procedure makes the calculations complicated. However, van Elp *et al.*[21] found that, at least in case of Ni^{2+} and Cr^{3+} in O_h symmetry, the discrepancy between the XAS taken at different orientations was small or even absent. In a first approximation we performed the calculations with the magnetic field along the crystallographic axes [001] (or C_4) assuming that this orientation well reproduces the isotropic XAS and XMCD spectra. The strength of the magnetic field is set to 0.3 meV corresponding approximately to the experimental magnetic field of 5 T.

TABLE I. Slater integrals and spin-orbit interactions used for the ligand field multiplet simulations of the Ni^{2+} and Cr^{3+} $L_{2,3}$ XAS edges. The Slater integrals are reduced of the 20% of the Hartree-Fock values to include the hybridization effects. All values are given in eV.

		Ni^{2+}		Cr^{3+}	
		Initial state $2p^63d^8$	Final state $2p^53d^9$	Initial state $2p^63d^3$	Final state $2p^53d^4$
Ligand field parameters	$10Dq$	1.5	1.5	2.1	2.1
	Ds	0	0	0	0
	Dt	0	0	0	0
Slater integrals	F^2_{dd}	9.787		8.622	9.277
	F^4_{dd}	6.078		5.404	5.816
	F^2_{pd}		6.177		5.221
	G^1_{pd}		4.630		3.830
	G^3_{pd}		2.633		2.178
s-o	ζ_{2p}		12.607		5.667
	ζ_{3d}	0.083	0.102	0.035	0.047

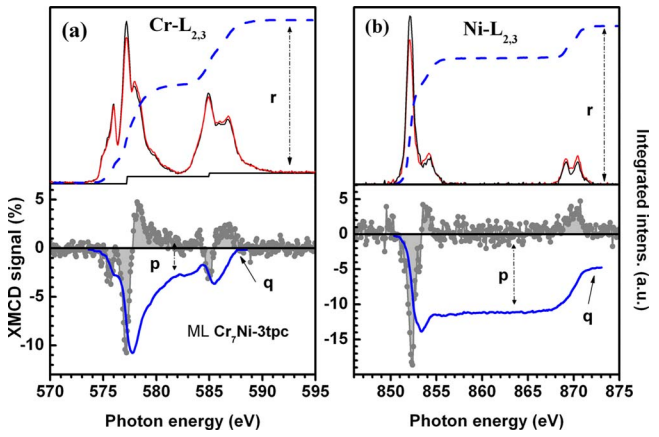

FIG. 4. (Color online) Upper panels: Cr (a) and Ni (b) $L_{2,3}$ XAS spectra taken with $\sigma^{\uparrow\uparrow}$ (black lines) and $\sigma^{\uparrow\downarrow}$ (red/gray lines) circularly polarized light and the XAS integral (dashed line) at 5 T and 10 K for Cr_7Ni-3tpc ML. Lower panels: XMCD spectra (dotted lines) and their integrals (continuous lines). The parameters p, q, and r are the values of the integrals used for the sum rules analysis.

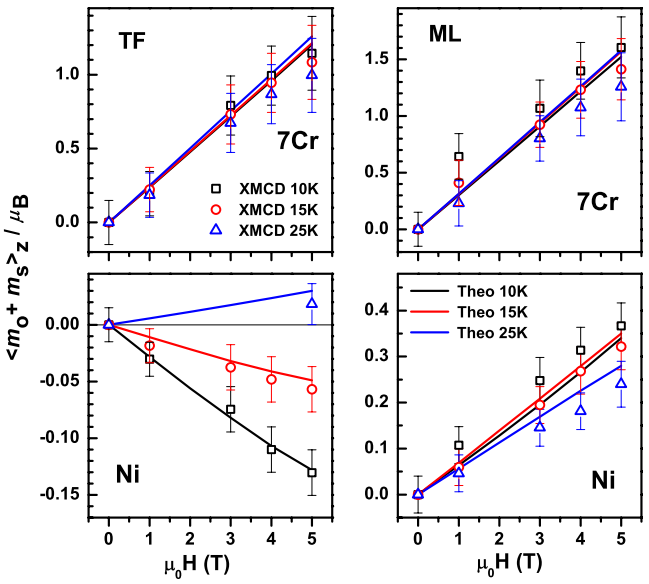

FIG. 5. (Color online) Cr_7Ni-3tpc TF (left panel) and sML (right panel). Cr and Ni total magnetic moments, experimentally derived by the sum rules, vs applied magnetic field at 10, 15, and 25 K compared with the results of the spin-Hamiltonian calculations. The magnetic moments uncertainty takes into account the signal-to-noise ratio of the spectrum from which it was derived.

C. Sum rules

Information on the nature of the intramolecular exchange interactions can be extracted from the study of the sign of the dichroic signal. Indeed, as an external magnetic field is applied we expect an interplay between the antiferromagnetic coupling between nearest-neighboring ions—favoring a staggered configuration of magnetic moments at low temperature—and the Zeeman interaction, that tends to align all magnetic moments along the field direction. The XMCD spectra, (Fig. 3) provide information on this interplay. The negative dichroic signal at the Cr L_3 edge and the positive one at the L_2 edge ($[L_3(-),L_2(+)]$ in short) imply that the total magnetic moment of Cr ions is parallel to **H**. This occurs for all TF and sML samples for all the monitored T and **H**. The opposite behavior [i.e., $L_3(+)$, $L_2(-)$] has been observed for Ni in all TFs, implying that the expected magnetic moment is antiparallel to **H** at 10 K, whereas for all sMLs the Ni magnetic moment is, in this case, parallel to **H**. While the sign of the Ni XMCD is the same in all the studied sMLs and opposite to that observed in bulk (TFs) samples, the intensity of the dichroic signal changes from one derivative to another (Fig. 3).

We have refined the above analysis by extracting the mean value of the spin (m_S) and orbital (m_O) moments (along the surface normal) for each kind of magnetic ion as a function of T by using XMCD sum rules.[16,22] In the following we focus on the Cr_7Ni-3tpc system which presents the largest differences between sML and TF, as representative of all the three derivatives. Figure 4 shows the Cr-$L_{2,3}$ and Ni-$L_{2,3}$ absorption spectra taken using both photon helicities (upper panel), the relative dichroic signal and its integral (lower panel) measured on the Cr_7Ni-3tpc sML at 10 K and 5 T. We used the same analysis successfully applied to thick films of Cr_8 and Cr_7Ni-piv,[16] and to which we refer for more details. The orbital (m_O) and spin (m_S) moment can be calculated by the following expressions:[22]

$$m_s/\mu_B = -\frac{(6p-4q)}{r} N_{\text{eff}} SC, \quad m_o/\mu_B = -\frac{4q}{3r} N_{\text{eff}},$$

where N_{eff}, the number of holes in the $3d$ shell, is equal to 7 and 2 for Cr^{3+} and Ni^{2+}, respectively. For Cr we derived a spin correction (SC) factor of 1.75.[16] Figure 4 shows the vanishing of the dichroic signal integral at the Cr-$L_{2,3}$ edges ($q=0$), that is m_O of the Cr^{3+} ions is completely quenched by the crystal field.[22] On the contrary m_O of Ni^{2+} ions is only partially quenched. This occurs for all TFs and sMLs investigated. For all systems the m_O value derived by the sum rules is of about 10% of m_S, for all spanned T and **H**. Thus Cr ions have a nearly spin-only gyromagnetic factor ($g_{\text{Cr}}=2.0$), whereas for Ni $g_{\text{Ni}}=2.2\pm0.1$, very close to the one derived for the Cr7Ni-piv system.[16] We may thus conclude that neither the functionalization nor the grafting onto the Au surface affects the degree of quenching of the orbital momentum.

Figure 5 displays the Cr and Ni total magnetic moments of the Cr7Ni-3tpc TF and sML, determined by the sum rules, as a function of μ_0**H** (up to 5 T) at different temperatures. The Cr total magnetic moment is larger in the sML than in the TF and it is always parallel to **H**, for all the T spanned. The opposite behavior is observed for Ni in TF: negative values, i.e., moment antiparallel to **H**, are observed at the lowest temperatures (10 and 15 K). The temperature increase, however, leads to an inversion of the sign of the Ni dichroism at 25 K, which is due to the alignment of the Ni magnetization to the external field, in analogy to what observed in Cr7Ni-piv TF.[16] Conversely, for the sML samples, the Ni magnetization is always positive (Fig. 5 lower right panel), i.e., the Ni total magnetic moment is aligned to **H**

already at $T=10$ K. This occurs for all three functionalizations studied here.

D. Comparison with the bulk and description by spin Hamiltonian

The behavior of the magnetic moments can be compared with that derived from bulk measurements. To do this we evaluated the mean value of the local magnetization for the Cr and the Ni ions by calculating the *eigenvalues* and *eigenstates* of the microscopic spin Hamiltonian describing each Cr_7Ni ring,

$$H = \sum_i J_{i,i+1}\mathbf{s}_i \cdot \mathbf{s}_{i+1} + \mu_B \mathbf{H} \cdot \sum_i g_i \mathbf{s}_i + H_{\text{ani}}, \qquad (1)$$

where the first term represents isotropic nearest-neighbor exchange and the second term is the Zeeman coupling to the external field **H**. Since XMCD results show that the degree of orbital momentum quenching is the same as in the original Cr_7Ni-piv molecule, gyromagnetic factors g_i have been fixed to 1.98 (Cr^{3+}) and 2.2 (Ni^{2+}).[10,11] H_{ani} represents small anisotropic terms. Since these play a secondary role in all the present discussion, they have been omitted for simplicity in the calculations. In order to assess independently the role of the functionalization and that of the molecule-to-substrate interaction we first analyzed the TF and then the sML. We extracted the exchange constant values from the simultaneous analysis of the TF's magnetic moments determined by sum rules (left panel of Fig. 5) and the low-temperature specific heat, ac susceptibility, and magnetization measured on Cr_7Ni-3tpc powders (see Fig. 6). The different data sets were found to be perfectly compatible and very well reproduced within the spin-Hamiltonian model using $J_{\text{Cr-Cr}} \sim 1.24$ meV and $J_{\text{Cr-Ni}} \sim 1.69$ meV. In particular, the comparison of calculated and XMCD derived magnetic moments is shown in Fig. 5 (left panel). Thus, the 3tpc functionalization itself induces a reduction by 15% of $J_{\text{Cr-Cr}}$ leaving unchanged the $J_{\text{Cr-Ni}}$ with respect to pristine Cr_7Ni-piv.[10,11] The larger response to the applied field characterizing grafted molecules points to a significant reduction in the antiferromagnetic exchange. Indeed, the sML experimental data in the right panels of Fig. 5 are well accounted by numerical simulations with $J_{\text{Cr-Cr}} \sim 1.05$ meV, $J_{\text{Cr-Ni}} \sim 0.5$ meV. The uncertainty on the TF and sML parameters is of the order of 10% as variations within this range keep the fit acceptable. Even if these parameters lead to a compression of the calculated energy levels spectrum [e.g., the ground-doublet to first-excited-quartet gap $\Delta_{1/2-3/2}$ becomes 0.7 meV (8 K); see Fig. 7], the low-E multiplet structure remains substantially the same as in the original Cr_7Ni-piv.[16] This implies that observation of quantum phenomena such as quantum oscillations described in Refs. 9 and 10 is not compromised. Moreover the energy gap between the $S=1/2$ and $S=3/2$, $\Delta_{1/2-3/2}$, is large enough to allow, for instance, efficient qubit encoding in the ground doublet,[11] and the quartet states can still be used as auxiliary resources for qubit manipulation.[12]

E. Discussion on the origin of exchange coupling variations

About the reason of the decrease in the exchange constants, much stronger for the $J_{\text{Cr-Ni}}$, when the molecule is put on the surface, it is unlikely that is associated with either breaking one of the two Cr-Ni edges within the ring or to direct interaction of the metals (Cr, Ni) with the gold surface. Both these two events should indeed significantly change the crystal environment of Cr and Ni ions resulting in clear changes in the absorption spectra, which were not observed (Fig. 3).

It is worth discussing the relation between the way molecules actually graft onto the surface, and the origin of the observed change in the exchange constants. From a quantitative analysis of the different MLs (see Fig. 3) we derived

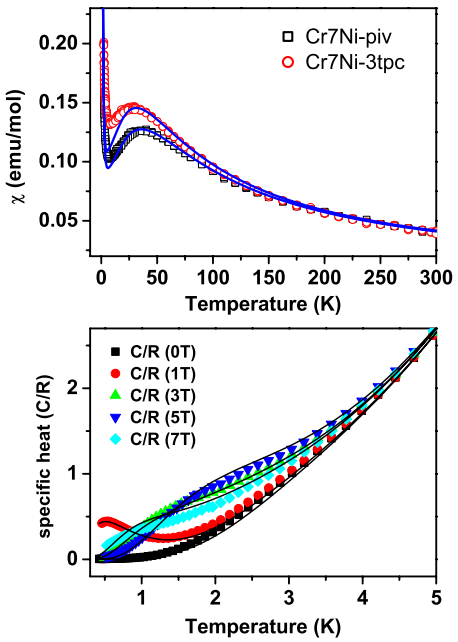

FIG. 6. (Color online) Top panel: ac susceptibility of the Cr_7Ni-3tpc powders compared with those of the Cr_7Ni-piv. Bottom panel: specific heat C, in $R=8.314$ J/mol K units, of Cr_7Ni-3tpc powders as a function of the temperature (T) and for several values of the applied magnetic field. Both measurements have been performed by a PPMS-7T system of Quantum Design. Continuous lines are fitting curves as resulting from the spin Hamiltonian simulations (see text).

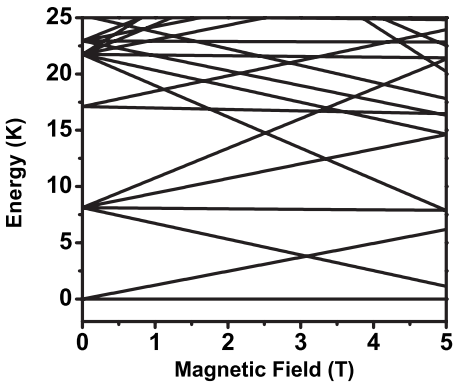

FIG. 7. Calculated field-dependence of the low-lying energy levels of Cr_7Ni-3tpc ML, relative to the ground-state energy. Parameters used in calculations are $J_{\text{Cr-Cr}}=1.05$ meV and $J_{\text{Cr-Ni}}=0.5$ meV.

that the magnitude of the normalized Ni XMCD signal for the 3tpc derivative (17%), is twice the value relative to the van der Waals interacting derivatives (including the single sulfur one). Let us notice that the entity of the ring distortion is not necessarily related to the proximity of Ni to the surface (length of the ligand), hence we do not expect any dispersion of the J values associated to it. Due to the local nature of the molecule-substrate bonding, which does not involve any charge transfer, a direct influence of the ligand-substrate bond on the metal core properties is not expected. This is true not only for van der Waals interactions but also for covalent S-Au bonds.[23] A confirmation that the "chemistry around the ligands" is negligible comes from the small change (15%) of the exchange constants for the TF when changing the piv ligand with the 3-tpc.

A possible explanation comes from a ring distortion with respect to the bulk conditions, simply due to the lack of the isotropic interactions with all the surrounding molecules. The resulting change in the overlap integrals yielding the superexchange paths explains the observed decrease in exchange constants with respect to their TF values. The fact that the stronger the ligand-substrate bonding, the higher the measured Ni dichroic signal, suggests that the distortion of the ring is modulated by the strains due to the ligands-substrate bonding. Density-functional calculations, reported in the following paragraph, show that for a small stretching of the ring structure, the $J_{\text{Cr-Cr}}$ is weakly perturbed while $J_{\text{Cr-Ni}}$ strongly decreases, in agreement with the experimental results.

F. Density-functional calculations

In order to elucidate the relationship between the J's changes and a possible ring distortion, we have performed state-of-the-art calculations of chain model system of Cr_8 by using the WIEN2K package,[24] which implements the all-electron augmented plane-wave method within spin-density functional theory. We used the generalized-gradient approximation of the exchange-correlation functional. In recent papers[25,26] we have demonstrated how the electronic and magnetic properties of the Cr_8 molecular magnet are well described by a infinite linear-chain model, where the cyclic structure of the original molecule is straightened, preserving bond angles and distances in the fluorine and carboxylate bridges. In Fig. 8 the chain model is sketched, and the parameters relevant for the discussion below explicitly indicated. The large computational gain achieved by using this model instead of the original cyclic structure allows us to perform extensive investigations on the dependence of the magnetic interactions as a function of the atomic distances and bond angle in the bridges. We have varied the Cr-Cr distance (d) above and below the experimental value (d_0 =3.39 Å), relaxing at each step the atomic positions of all the atoms in the bridges toward their equilibrium positions. We have performed this structural minimization for the antiferromagnetically coupled Cr chain. Once the atomic positions are optimized for a certain Cr-Cr distance, we could substitute one of the two inequivalent Cr atom with a Ni atom (neutralizing the negatively e^- charged cell by a positive jellium charge), characterizing thus an alternating Cr-Ni chain; keeping the atomic position unaltered upon Ni substitution is consistent with the fact that Cr_7Ni molecules are isostructural to Cr_8. Finally, by total energy calculations of the ferromagnetic and antiferromagnetic configuration of the pure Cr and Cr-Ni alternating chains, we could extract the Heisenberg exchange parameters Js describing the Cr-Cr and Cr-Ni magnetic couplings.

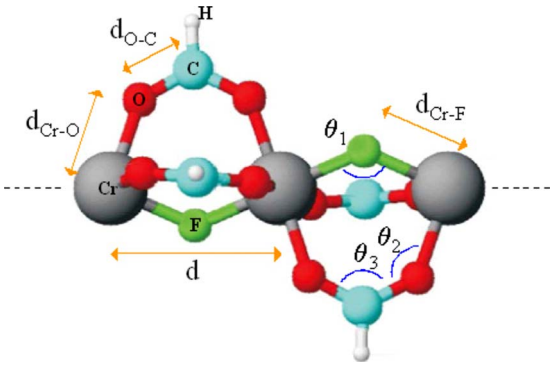

FIG. 8. (Color online) The chain model used in the calculations; relevant parameters such as Cr-Cr, Cr-F, Cr-O, and O-C distances, as well as Cr-F-Cr, Cr-O-C, and O-C-O angles characterizing the bridges and the dilation of the molecule are depicted as well.

In Fig. 9 we present the variation in $J_{\text{Cr-Cr}}$ and $J_{\text{Cr-Ni}}$ (normalized to their values for the undilated structure, J_0s) as a function of d (top panel) and we show how the bond distances (central panel) and angles (bottom panel) varies upon variation in d. In a range of dilation of the Cr-Cr (Cr-Ni) distance up to 7% (which is supposed to cover the possible experimental range of dilation of an isolated molecule as compared to a molecule packed in a molecular crystal), $J_{\text{Cr-Ni}}$ is found to vary more sensibly compared to $J_{\text{Cr-Cr}}$. For instance, supposing a dilation of 5%, $J_{\text{Cr-Cr}}$ and $J_{\text{Cr-Ni}}$ assume values which are, respectively, 29% and 60% smaller as compared to the J_0s of the undilated structure. These variations are completely consistent with the ones inferred from experimental data. Since, as evidenced in Fig. 9, distances between atoms in the bridges remain more or less unvaried while angles are primarily influenced in a linear way when stretching or compressing the Cr-Cr distance, a similar paraboliclike variation in Js could also be obtained when plotting the Js as a function of the bond angles (not shown). The different behaviors of the Cr-Cr and Cr-Ni exchange parameters as a function of the bond angles, as well as the relative contribution of the carboxylate and fluorine bridges will deserve further analysis and will be the subject of a future investigation. We note in passing that a parabolic behavior of the magnetic coupling between two Cr moments as a function of the bond angles has been already observed in case of hydroxo doubly bridged Cr dimers.[27]

IV. CONCLUSIONS

In summary we found that the electronic properties (high energy scales) of molecular Cr7Ni rings are the same for thick films and submonolayer samples, whereas the magnetic properties (reflecting low-energy scales) are somewhat dif-

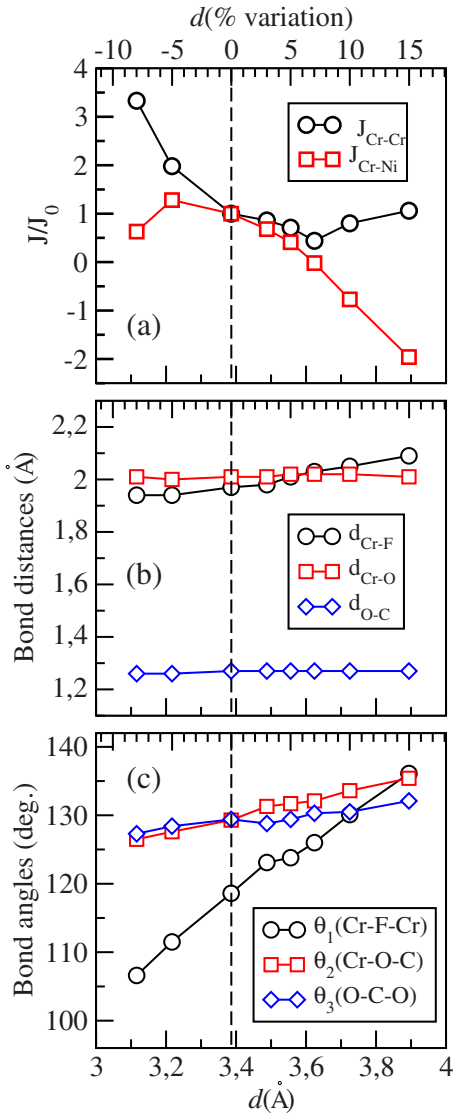

FIG. 9. (Color online) (a) Variation in the exchange parameters as a function of the Cr-Cr (Cr-Ni) distance d. The $J_{\text{Cr-Cr}}$ and $J_{\text{Cr-Ni}}$ have been normalized to the J_0 values calculated for the undilated d_0 distance. Variation in the bond distances (b) and bond angles (c) in the fluorine and carboxylate bridges as a function of the Cr-Cr (Cr-Ni) distance d.

ferent. Unlike the case with the most popular Mn_{12} single molecule magnet, we found that molecular Cr_7Ni rings are chemically robust, allowing the low-E multiplet structure to remain substantially the same as in the original bulk Cr_7Ni-piv. This conclusion is supported by comparison with spin-Hamiltonian simulations. Density-functional theory (DFT) calculations clarify that a small distortion of the rings is enough to explain the change of the $J_{\text{Cr-Ni}}$ exchange coupling, which actually results weaker than the $J_{\text{Cr-Cr}}$ within the rings. After the submission of this work, we learned about similar results obtained in submonolayer of molecular Fe_4 deposited by liquid phase on gold surface.[28] We believe that these two independent results show that some complex magnetic molecules can be safely grafted on surfaces without drastic chemical changes, while some little changes may occur in their magnetic features. This conclusion is a fundamental step forward in the field and it paves the way to the addressing of single molecules anchored on surface.

ACKNOWLEDGMENTS

This work has been carried out within the framework of the EU Contracts "MAGMANet" Grant No. 515767, FP7-ICT "MolSpinQIP" Grant No. 211284 and supported by the PRIN Grant No. 2006029518 (IT) and EPSRC (UK). We acknowledge the European Synchrotron Radiation Facility for provision of synchrotron radiation facilities and we would like to thank Julio Criginsky Cezar for assistance in using beamline ID8.

APPENDIX: SYNTHETIC PROCEDURE

The synthetic procedure of the Cr_7Ni-3-thiophenecarboxylate [Fig. 1(b)] $[NH_2^nPr_2][Cr_7NiF_8(3\text{-tpc})_{16}]$ is described in Ref. 15, while the Cr_7Ni-3-phenoxybenzoate [Fig. 1(d)] $[(\mathbf{C_3H_7})_2\mathbf{NH_2}][\mathbf{Cr_7NiF_8}(\boldsymbol{m}\text{-}\mathbf{C_6H_5OC_6H_4CO_2})_{16}]$ was obtained in a similar procedure to compound Cr_7Ni-3tpc (2) by using 3-phenoxybenzoic acid instead of the thiophene-3-carboxylic. The product was crystallized from acetone/acetonitrile. Yield: 60% (based on Cr). Elemental analysis calculated for $Cr_7NiC_{214}H_{160}O_{48}NF_8$: Cr, 8.90; Ni, 1.44; C, 62.87; H, 3.94; N, 0.34. Found: Cr, 9.04; Ni, 1.48; C, 62.92; H, 3.80; N, 0.31. Synthetic procedure of the Cr_7Ni-4-(methylthiophenyl)propionate [Fig. 1(c)]. The $[Cr_7NiF_8\ (CH_3)_3\ CCH_2COO)_{15}\ (CH_3SC_6H_4CH_2CH_2COO)]$ $[H_2N(CH_2CH_3)_2]$: $[Cr_7NiF_8(CH_3)_3CCH_2COO)_{16}]$ $[H_2N(CH_2CH_3)_2]$ (0.298 g, 0.120 mmol) and 3-(4-methylthiophenyl) propionic acid (0.118 g, 0.601 mmol) were combined in acetonitrile (10 mL). The resulting mixture was refluxed for 25 h and stirred at room temperature for a further 56 h. The volume was reduced to dryness, and the resulting green product was redissolved in hexane. The solution was purified by column chromatography in 9:1 hexane:ethyl acetate, with the titled product eluting as the second band. The product was recrystallized using acetonitrile (yield 84 mg, 27%). MS (ES^+, m/z) 2594 (M+Na), 2644 [M $+H_2N(CH_2CH_3)_2$]}.

*valdis@unimore.it

[1] D. Gatteschi, R. Sessoli, and J. Villain, *Molecular Nanomagnets* (Oxford University Press, New York, 2007).

[2] H. Wende, M. Bernien, J. Luo, C. Sorg, N. Ponpandian, J. Kurde, J. Miguel, M. Piantek, X. Xu, Ph. Eckhold, W. Kuch, K. Baberschke, P. M. Panchmatia, B. Sanyal, P. M. Oppeneer, and O. Eriksson, Nature Mater. **6**, 516 (2007).

[3] A. Cornia, A. C. Fabretti, M. Pacchioni, L. Zobbi, D. Bonacchi,

A. Caneschi, D. Gatteschi, R. Biagi, U. del Pennino, V. De Renzi, L. Gurevich, and H. S. J. Van der Zant, Angew. Chem., Int. Ed. **42**, 1645 (2003).
[4] L. Bogani, L. Cavigli, M. Gurioli, R. L. Novak, M. Mannini, A. Caneschi, F. Pineider, R. Sessoli, M. Clemente-León, E. Coronado, A. Cornia, and D. Gatteschi, Adv. Mater. **19**, 3906 (2007).
[5] M. Mannini, P. Sainctavit, R. Sessoli, C. Cartier dit Moulin, F. Pineider, M.-A. Arrio, A. Cornia, and D. Gatteschi, Chem.-Eur. J. **14**, 7530 (2008).
[6] E. Coronado, A. Forment-Aliaga, F. M. Romero, V. Corradini, R. Biagi, V. De Renzi, A. Gambardella, and U. del Pennino, Inorg. Chem. **44**, 7693 (2005).
[7] S. Voss, M. Fonin, U. Rüdiger, M. Burgert, U. Groth, and Yu. S. Dedkov, Phys. Rev. B **75**, 045102 (2007).
[8] Z. Salman, K. H. Chow, R. I. Miller, A. Morello, T. J. Parolin, M. D. Hossain, T. A. Keeler, C. D. P. Levy, W. A. MacFarlane, G. D. Morris, H. Saadaoui, D. Wang, R. Sessoli, G. G. Condorelli, and R. F. Kiefl, Nano Lett. **7**, 1551 (2007).
[9] S. Carretta, P. Santini, G. Amoretti, M. Affronte, A. Ghirri, I. Sheikin, S. Piligkos, G. Timco, and R. E. P. Winpenny, Phys. Rev. B **72**, 060403(R) (2005).
[10] S. Carretta, P. Santini, G. Amoretti, T. Guidi, J. R. D. Copley, Y. Qiu, R. Caciuffo, G. Timco, and R. E. P. Winpenny, Phys. Rev. Lett. **98**, 167401 (2007).
[11] F. Troiani, A. Ghirri, M. Affronte, S. Carretta, P. Santini, G. Amoretti, S. Piligkos, G. Timco, and R. E. P. Winpenny, Phys. Rev. Lett. **94**, 207208 (2005).
[12] F. Troiani, M. Affronte, S. Carretta, P. Santini, and G. Amoretti, Phys. Rev. Lett. **94**, 190501 (2005).
[13] F. K. Larsen, E. J. L. McInnes, H. El Mkami, J. Overgaard, S. Piligkos, G. Rajaraman, E. Rentschler, A. A. Smith, G. M. Smith, V. Boote, M. Jennings, G. A. Timco, and R. E. P. Winpenny, Angew. Chem., Int. Ed. **42**, 101 (2003).
[14] M. Affronte, F. Troiani, A. Ghirri, S. Carretta, P. Santini, V. Corradini, R. Schuecker, C. Muryn, G. Timco, and R. E. Winpenny, Dalton Trans. **2006**, 2810 (2006).
[15] V. Corradini, R. Biagi, U. del Pennino, V. De Renzi, A. Gambardella, M. Affronte, C. A. Muryn, G. A. Timco, and R. E. P. Winpenny, Inorg. Chem. **46**, 4937 (2007).
[16] V. Corradini, F. Moro, R. Biagi, U. del Pennino, V. De Renzi, S. Carretta, P. Santini, M. Affronte, J. C. Cezar, G. Timco, and R. E. P. Winpenny, Phys. Rev. B **77**, 014402 (2008), and references therein.
[17] E. Gaudry, P. Sainctavit, F. Juillot, F. Bondioli, P. Ohresser, and I. Letard, Phys. Chem. Miner. **32**, 710 (2006).
[18] M.-A. Arrio, A. Scuiller, P. Sainctavit, Ch. Cartier dit Moulin, T. Mallah, and M. Verdaguer, J. Am. Chem. Soc. **121**, 6414 (1999).
[19] B. T. Thole, G. van der Laan, J. C. Fuggle, G. A. Sawatzky, R. C. Karnatak, and J.-M. Esteva, Phys. Rev. B **32**, 5107 (1985); B. T. Thole, G. van der Laan, and P. H. Butler, Chem. Phys. Lett. **149**, 295 (1988).
[20] F. M. F. de Groot, J. Electron Spectrosc. Relat. Phenom. **67**, 529 (1994); Chem. Rev. **101**, 1779 (2001).
[21] J. van Elp and B. G. Searle, J. Electron Spectrosc. Relat. Phenom. **86**, 93 (1997).
[22] C. T. Chen, Y. U. Idzerda, H. J. Lin, N. V. Smith, G. Meigs, E. Chaban, G. H. Ho, E. Pellegrin, and F. Sette, Phys. Rev. Lett. **75**, 152 (1995).
[23] V. De Renzi, R. Rousseau, D. Marchetto, R. Biagi, S. Scandolo, and U. del Pennino, Phys. Rev. Lett. **95**, 046804 (2005).
[24] P. Blaha *et al.*, WIEN2K, An Augmented Plane Wave+Local Orbitals Program for Calculating Crystal Properties (Karlheinz Schwarz, Techn. Universität Wien, Austria, 2001). For further details visit the web page: http://www.wien2k.at
[25] D. M. Tomecka, V. Bellini, F. Troiani, F. Manghi, G. Kamieniarz, and M. Affronte, Phys. Rev. B **77**, 224401 (2008).
[26] V. Bellini, A. Olivieri, and F. Manghi, Phys. Rev. B **73**, 184431 (2006).
[27] O. Castell and R. Caballol, Inorg. Chem. **38**, 668 (1999).
[28] M. Mannini, F. Pineider, Ph. Sainctavit, C. Danieli, E. Otero, C. Sciancalepore, A. M. Talarico, M. A. Arrio, A. Cornia, D. Gatteshi, and R. Sessoli, Nature Mater. **8**, 194 (2009).